Global Horizontal Irradiance and Meteorological Parameters Analysis for Modeling Effects of Cloud Motion on PV Generation

Shaimaa Omran*‡, Murat Dilek **, Robert Broadwater ***

* Engineering Research Division, National Research Centre, El Buhouth st., Dokki, Cairo,12622, Egypt

**Electrical Distribution Design (EDD), Blacksburg, VA 24061 USA

***Electrical and Computer Engineering Department, Virginia Tech, Blacksburg, VA 24061, USA

(s.a.omran@ieee.org, murat-dilek@edd-us.com, dew@vt.edu)

‡ Corresponding Author; Shaimaa Omran, Engineering Research Division, National Research Centre, El Buhouth st., Dokki, Cairo,12622, Egypt, Tel: +201067813566, s.a.omran@ieee.org

Received: 05.02.2020 Accepted:01.03.2020

Abstract- Efforts are exerted worldwide to increase the deployment of renewables specifically solar photovoltaic (PV) systems. One main challenge to face is the perturbation due to the fluctuating nature of the solar energy. The intermittency of the irradiance received by the solar PV systems is mainly caused by the cloud covering the PV system. In this paper a statistical analysis of the received Global Horizontal Irradiance (GHI) by a real PV plant as well as the meteorological conditions/parameters surrounding the PV arrays is performed. The results for the GHI analysis shows that the relative change of GHI over the period of the study is 70% or less for 63.32% of the time. Moreover, the GHI decay duration is equal to 20 seconds or less for 68.07% of the time for the study period. The meteorological data analyzed include the speed of the cloud, gust, number of clouds passing, width of the clouds, and the time interval between consecutive clouds. Detailed numeric results are obtained and depicted for these parameters over the time period set for the study. One objective of this study is to indicate and adjust the parameters that are to be fed to a Cloud Motion Simulator (CMS); which is a software that simulates the repeated passage of clouds over an electric power system model which includes interconnected PV.

Keywords Global horizontal irradiance, meteorological parameters, cloud cover, photovoltaic power.

1. Introduction

According to the Renewables 2019 Global Status Report the solar photovoltaic (PV) power continued dominating the investments for renewable energy resources in 2018, the investments accounted for 48% of the total renewables investments. This is depicted in Fig. 1. The investment commitments for solar power in 2018 was $139.7 billion. The trends for the global investment in renewables in 2019 was $45.4 billion in the first quarter of 2019. Several cities worldwide are exerting efforts to increase the deployment of renewables. One reason is to provide a cheaper and more stable alternative to imported fuels, reducing CO_2 harmful emissions and other pollutants [1]. Furthermore, about 100 GW PV plants were installed in 2018 which is about 55% of the total global renewables capacity installations of 181 GW. In addition to the increased investments and installations of renewables and specifically PV, there is also a significant increase in researching this area [2-4]. Various factors studied that affect the output power of PV modules include dust [5, 6], rise in temperature of PV cells [7, 8], depreciation of cells over time[9] and of course clouds. Recently, a lot of research in the literature addressed forecasting and predicting the solar irradiance as it is considered the primary information for designing and assessing PV systems [10-15]. Moreover, many studies investigated the performance of photovoltaic (PV) power systems under real meteorological conditions, analyzing and modelling the solar irradiance and other

meteorological parameters [16-18]. Furthermore, it is declared in [19] that clouds can significantly limit the PV power generation; specifically it is mentioned that in 45 seconds it can drop to 90%. Thus, several studies investigated and considered the impact of cloud covers and shading on the GHI irradiance values and accordingly on PV system intermittency [20-31]. For example, [20] proposed a prediction model for a PV system output based on a cloud model. This model is developed taking into consideration environmental factors such as the temperature, humidity, and radiation intensity. Moreover, [21] investigated the effect of large variations in PV power under cloud cover and low-voltage-ride-through on the power grid of a real system. In addition, [26] presented a PV generation parametric modelling that relies on raw data for the cloud cover obtained from meteorological resources incorporated with electrical power generation measurements. This model can be implemented when integrating large-scale PV plants within the grid. Furthermore, [22] proposed a geometric technique to determine the clouds speed and direction based on high resolution sky images projected over the PV panels. Thus, tracking the cloud from the moment it approaches the PV panel till it leaves it. Also, [27] used real sky images to determine the cloud cover distribution and its characteristics concerning light transmission. This was in turn used to develop an irradiance profile on the surface of inclined PV panels within a real PV plant. This studies aimed to estimate precisely the fluctuations of the PV power and accurately determine the exact PV output. In the present work, field data from a real system is used to conduct an analysis of the clouds passing over a solar PV array in Brookhaven, New York and determine how these clouds impact the received irradiance by the PV plant [32]. A statistical analysis of the received irradiance by this PV plant as well as the meteorological conditions/parameters surrounding the PV arrays is performed. The meteorological data analyzed include the speed of the cloud, gust, number of clouds passing, width of the clouds, and the time interval between consecutive clouds. One main contribution of this study is to indicate/calibrate/adjust the parameters that are to be fed to a Cloud Motion Simulator (CMS); which is the software that simulates the repeated passage of clouds over a distribution model and interconnected PV. The CMS simulates the effects of cloud shadows on PV systems, and the consequent voltage fluctuations in a quasi-steady-state fashion [33, 34]. Another main contribution of the study is performing the analysis on a real life system using field data to be able to obtain precise estimates of the PV output of this plant under real cloudy weather conditions. It is also worth mentioning that the GHI measured data over the PV panels in the 1 MW PV power plant in Brookhaven, New York, is 1 second recorded data rather than data recorded in the range of minutes used in previous studies. The remainder of the paper is organized as follows. Section 2 defines describes what the CMS. Section 3 presents the data collection and methods used for analyzing the global horizontal irradiance (GHI) and meteorological parameters. Section 4 is devoted to results and discussion of the analysis. Finally, section 5 concludes the paper.

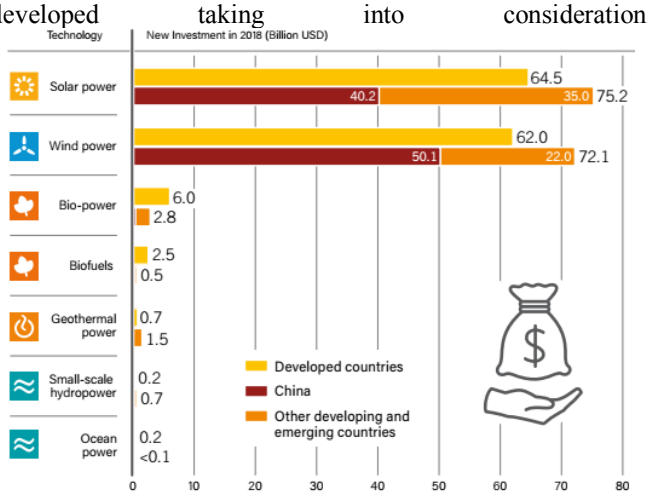

Fig. 1. Developed countries new investments in renewables in 2018[1]

2. Cloud Motion Simulator

The effect of cloud shadows on PV generation and its consequent impact on power systems may be simulated and studied using several methods. Some studies have simulated the cloud shadow effect using step changes[35, 36]. In the step change technique two power-flows are conducted, one at the beginning to determine the state of a system and the other for determining the final state. Then, the difference between the two states is calculated. In step-change tests a sudden drop in PV inverter output power is experienced when a cloud covers the PV systems, and in the same fashion, the inverter output returns to the initial value, or to a new value, after the cloud passes away. In other studies an assumption that the cloud is covering all the PV generators is used to simulate the system. These are two non-realistic assumptions that should be handled. The Cloud Motion Simulator (CMS) conducts a more precise simulation of the PV generation fluctuations due to cloud shadows using quasi-steady state simulations. In these simulations steady state models are used; nevertheless, the inputs (whether generation or loads) will change from one steady state solution to the other. This implies that clouds affecting a particular section of the PV system can be monitored and tracked. Moreover, the direction of the motion of the clouds can be detected and considered in the simulation [33, 34]. In this research the cloud simulation needs specific, detailed meteorological data. Analysis of solar irradiance, global horizontal irradiance (GHI), and meteorological data is presented in the following sections for a real PV system.

3. GHI and Meteorological Parameters Analysis

The output of the PV plant is represented by solar irradiation measured by solar resource instrumentation at multiple locations within the array. Data was obtained in the form of 12 text files for 12 months for the year 2013. Each file includes 1 second recorded data of the Global Horizontal Irradiance (GHI) measured over the PV panels in the 1 MW PV power plant. The text files were converted to database files for running queries required for the study.

After the pre-processing of the data files and performing the queries, the following stage was plotting the data. As 1 second recorded data for 12 months was a huge amount of data

to plot, one month was chosen from each season to plot its corresponding measurements. Meteorologists divide the year into 4 meteorological seasons of 3 months each:

- Spring - from March 1 to May 31;
- Summer - from June 1 to August 31;
- Fall (autumn) - from September 1 to November 30; and,
- Winter - from December 1 to February 28 (February 29 in a leap year) [37].

The mid-month of each season was chosen as representative of the season. Thus the authors plotted the 1 second GHI measured data for April, July, October, and January for the year 2013. Days with variations in GHI values were spotted and variations (decay and recovery) were coloured for elaboration. Sample plots for selected durations of selected days from the four months are depicted in the following figures. Fig. 2 and Fig. 3 present variations in GHI values measured on January 23, 2013 at 11:05:00 to 11:15:59, and April 14, 2013 at 09:46:00 to 09:59:59 respectively.

3.1. GHI relative % change

The normalized relative % changes for GHI values were calculated. Assuming the GHI values drops from GHI_i to GHI_j and then recovers once more to reach GHI_k, as shown in Fig. 4, then the Decay Normalized Relative % change (DNR) and the Recovery Normalized Relative % change (RNR) can be calculated using the following equations, respectively.

$$DNR\ \% = \frac{|\ GHI_j - GHI_i\ |}{GHI_M} \quad (1)$$

$$RNR\ \% = \frac{GHI_k - GHI_j}{GHI_M} \quad (2)$$

where GHI_M is the maximum GHI value observed over the current hour.

The values of the DNR% and RNR% are both referred to as the GHI normalized relative % changes. These % changes are evaluated for each of the 4 chosen months and a statistical analysis performed. The changes were categorized/divided into classes/ranges, and then a histogram plot representing the frequency of each GHI normalized relative % change range was plotted. The mean and standard deviation of the normalized relative % change values were used to calculate the Probability Density Function (PDF) and the Cumulative Distribution Function (CDF). The PDF presents the probability of a normalized relative % change value occurring. The CDF indicates the probability that a certain normalized relative % change value is equal or less than a specified value.

The Matlab® Statistics and Machine Learning Toolbox built in functions "pdf" and "cdf" shown below were used and yielded the presented results.

P = pdf('Normal', x, μ, σ);

C = cdf('Normal', x, μ, σ);

where **'Normal'** refers to the name of the distribution used, **x** is a vector of the GHI normalized relative % changes, **μ** is the average value, and **σ** is the standard deviation.

The statistical formulas used for the PDF and the CDF calculations are as follows.

The probability density function (PDF) is:

$$f(x) = \frac{1}{\sigma\sqrt{2\,\pi}}\, e^{\frac{-(x-\mu)^2}{2\sigma^2}}\ ,\sigma > 0 \quad (3)$$

The cumulative distribution function is:

$$F(x) = \int_{-\infty}^{x} \frac{1}{\sigma\sqrt{2\,\pi}}\, e^{\frac{-(t-\mu)^2}{2\sigma^2}}\ dt\ ,\sigma > 0 \quad (4)$$

where μ is the mean, σ is the standard deviation, and σ^2 is the variance.

3.2. GHI decay duration

The decay duration is the time taken for the GHI curve to drop from point GHI_i to point GHI_j before starting to recover as shown in Fig. 4. The values of the decay durations for each of the 4 chosen months are evaluated. They are categorized into ranges and then the histogram plot, which represents the frequency of each decay duration range, is plotted. The mean and standard deviation of the decay duration values are used to calculate the PDF and the CDF.

3.3. Meteorological parameters analysis

The CSM meteorological parameters are analyzed in this section, including the mean speed of the cloud, the cloud gust, the number of clouds passing each hour, the width of the clouds, and the time interval between consecutive clouds are analyzed in this section.

The length and width of the cloud are parameters that should be incorporated into the analysis. In the CMS the cloud is simulated as a rectangle with a length equal to the widest side of the circuit in the direction of the cloud motion [33, 34], where the width of the cloud can be set to a measured value. The width of the cloud can be estimated roughly using the decay duration and the average cloud/wind speed as follows:

Cloud Width (feet) =

decay duration (sec) x mean cloud speed (feet/sec) (5)

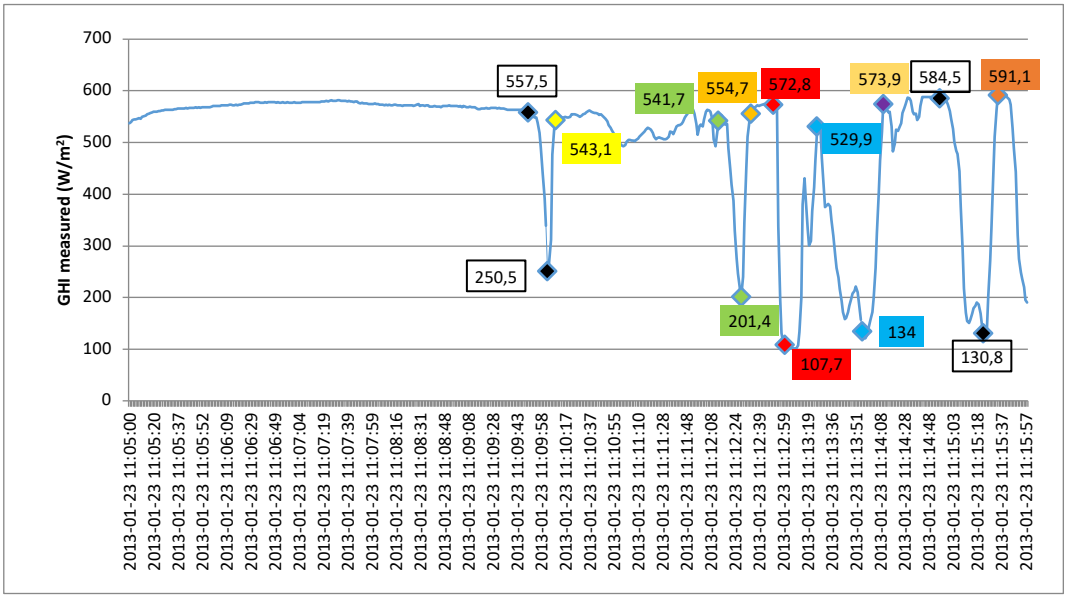

Fig. 2. January variations in GHI values measured on 01/23/2013 at 11:05:00 - 11:15:59

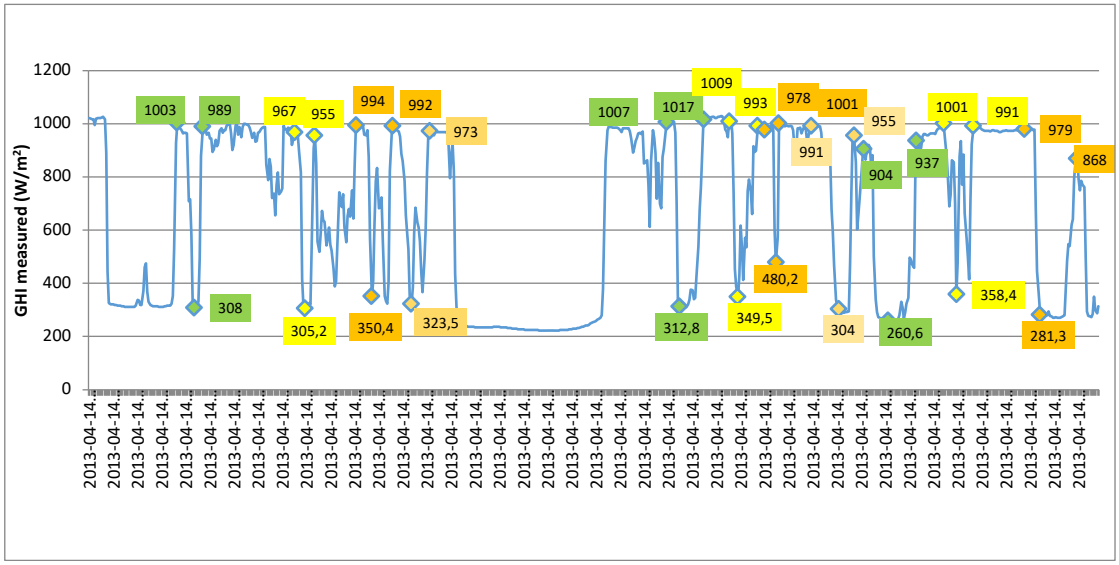

Fig. 3. April variations in GHI values measured on 04/14/2013 at 09:46:00 - 09:59:59

4. Results and Discussion

4.1. GHI relative % change analysis results

The histogram, the cumulative density function (CDF) and the probability density function (PDF) for the GHI normalized relative % change calculated values are depicted for each of the 4 months in Fig. 5 to Fig. 8. It is observed that the dominant (most frequent) value of the GHI relative % change for January, July and October is in the range of 70% to 80%. Whereas, the dominant (most frequent) value of the GHI relative % change for April is in the range of 60% to 70%.

It is noted that July has the worst GHI relative % change which is equal to 80% or less for 98.59% of the time. The GHI relative % change value with the highest PDF for July is 62.5%. April has the lowest value for GHI relative % change among the 4 months which is 70%, or less for 82.64% of the time. The GHI relative % change with the highest PDF for April is 61.4%. It is worth noting that the GHI relative % change with the highest PDF for October is 70.30%.

When combining the GHI normalized relative % change for the 4 months and plotting them we get a most frequent GHI normalized relative % change in the range of 70% to 80%. The relative change of GHI for the 4 months combined is 70% or less for 63.32% of the time, and this is depicted in Fig. 9(a). In Fig. 9(b) it is shown that the GHI normalized relative % change with the highest PDF for the 4 months combined is 64.26%.

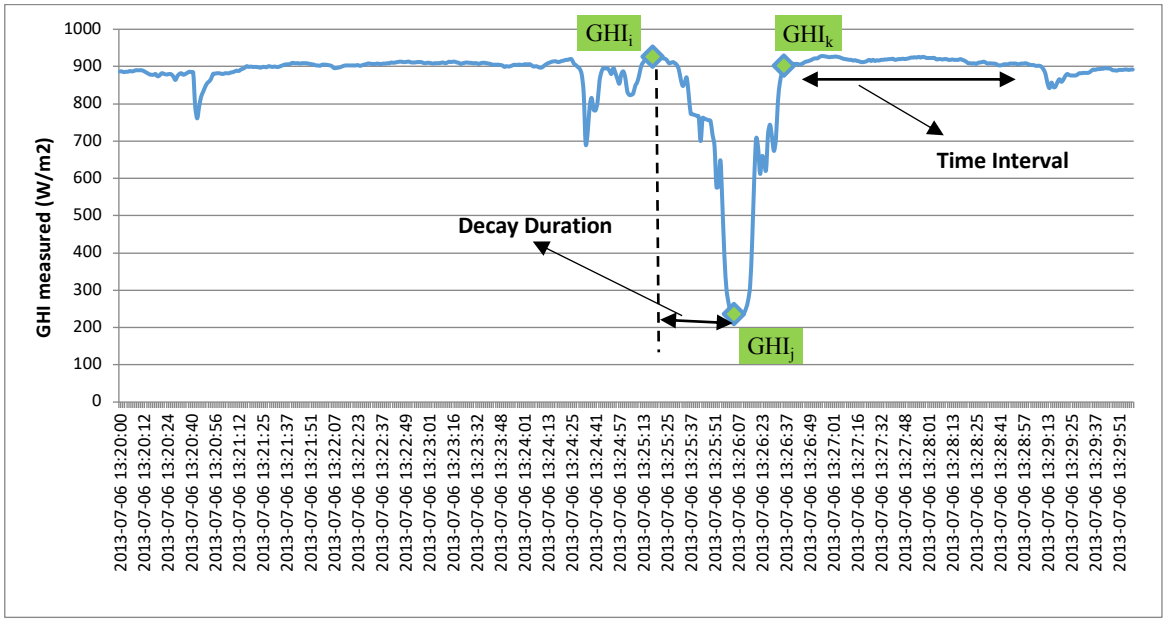

Fig. 4. Variations in GHI values measured over a specified time interval

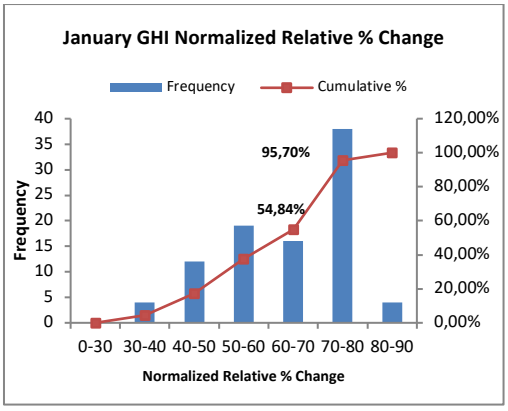

(a)

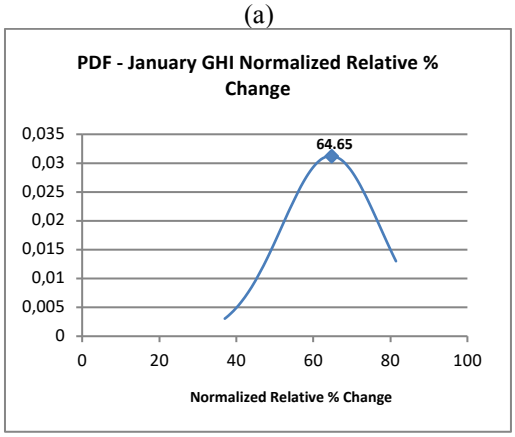

(b)

Fig.5. January GHI normalized relative % change (a) CDF and Frequency (b) PDF

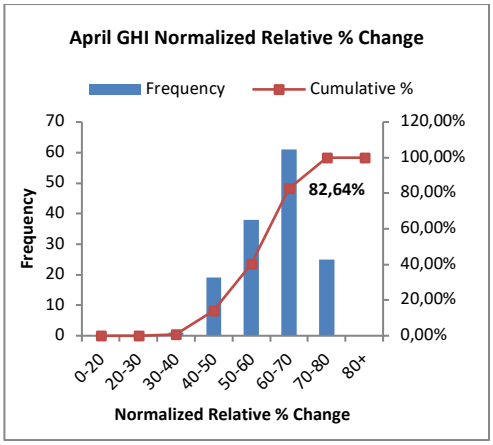

(a)

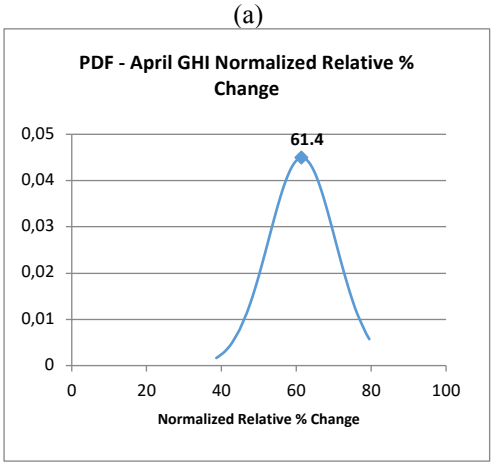

(b)

Fig. 6. April GHI normalized relative % change (a) CDF and Frequency (b) PDF

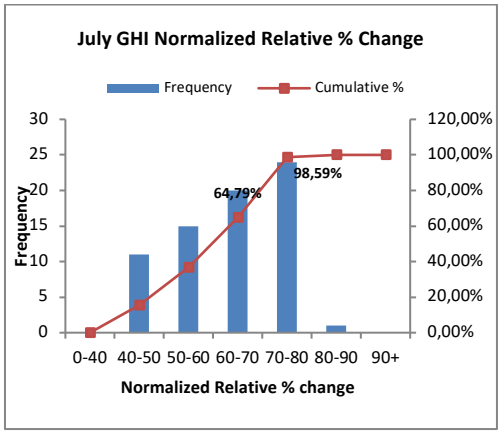

(a)

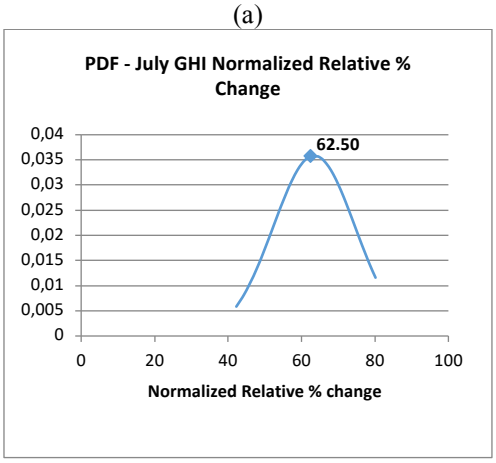

(b)

Fig. 7. July GHI normalized relative % change (a) CDF and Frequency (b) PDF

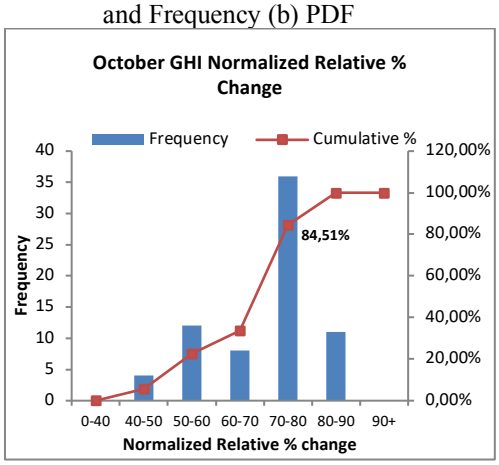

(a)

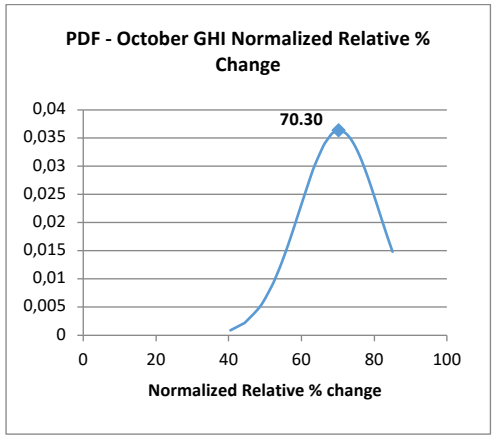

(b)

Fig. 8. October GHI normalized relative % change (a) CDF and Frequency (b) PDF

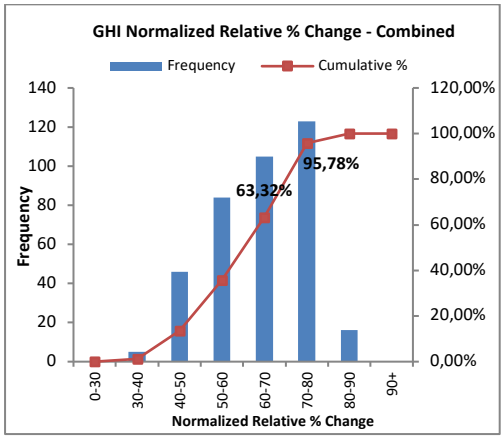

(a)

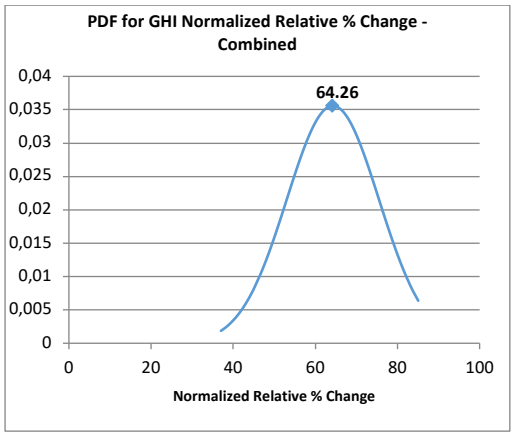

(b)

Fig. 9. The four months combined GHI normalized relative % change (a) CDF and Frequency (b) PDF

4.2. GHI decay duration analysis results

The histogram, the CDF, and the PDF for the GHI decay duration calculated values are depicted for each of the 4 months in Fig. 10 to Fig. 13. It is observed that the most frequent decay duration time for January and July is in the range of 10 to 15 seconds, whereas for April and October it is in the range of 5 to 10 seconds. It is shown in Fig. 14(a) that when combining the GHI decay duration values for the 4 months and plotting them we get a most frequent GHI decay duration values in the range of 10 to 15 seconds.

The GHI decay duration is equal to 20 seconds or less for 68.07% of the time for the 4 months combined. In Fig. 14(b) it is shown that the GHI decay duration for the 4 months with highest PDF value is 19 seconds. Table 1 shows a brief comparison of the GHI analysis results for the different months of the study.

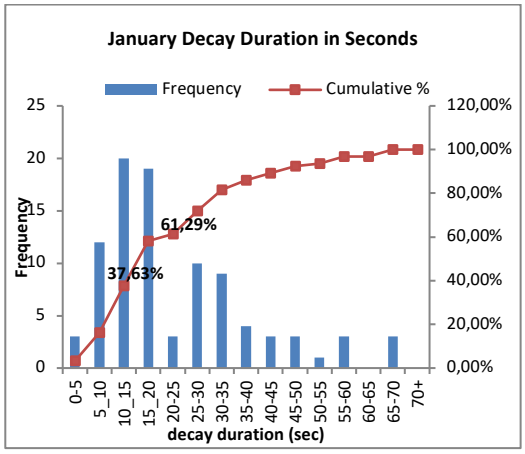

(a)

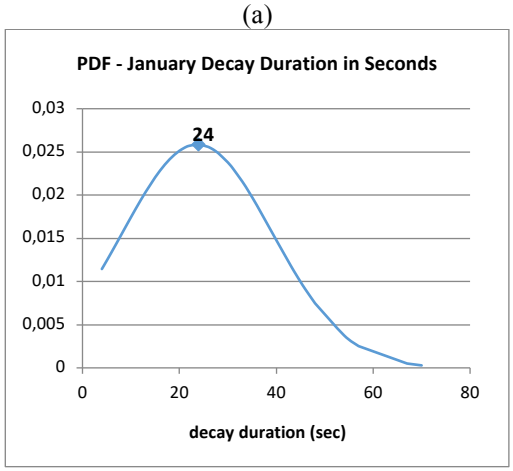

(b)

Fig. 10. January GHI decay duration values in seconds (a) CDF and Frequency (b) PDF

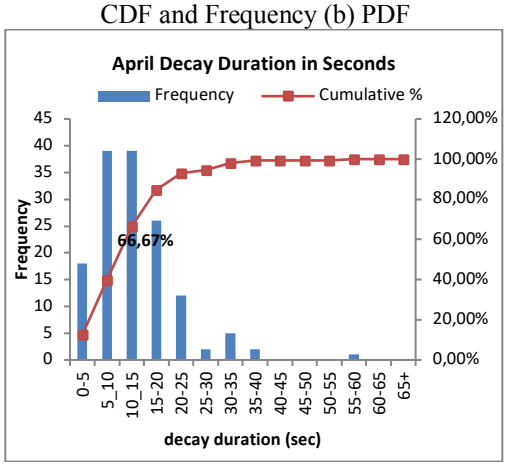

(a)

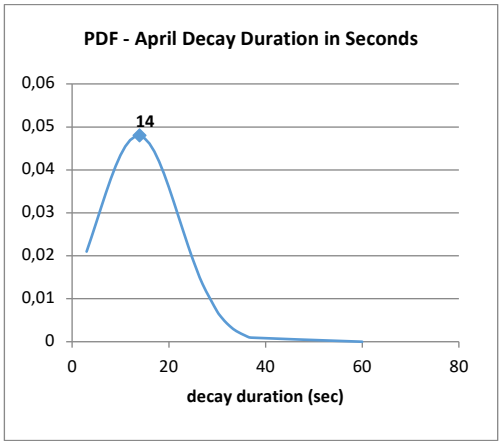

(b)

Fig. 11. April GHI decay duration values in seconds (a) CDF and Frequency (b) PDF

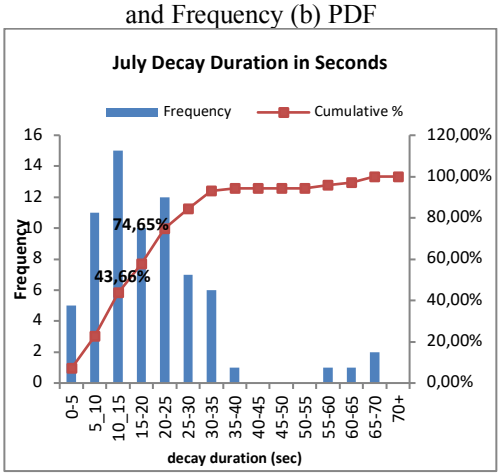

(a)

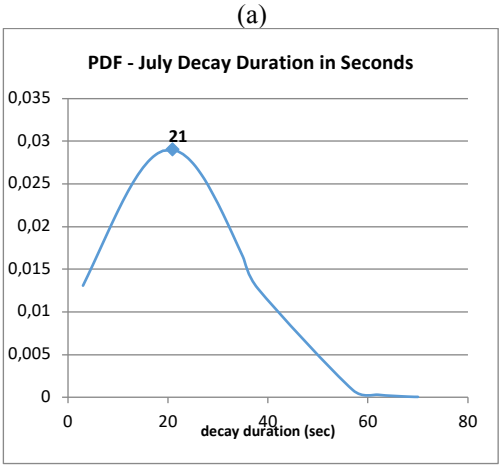

(b)

Fig. 12. July GHI decay duration values in seconds (a) CDF and Frequency (b) PDF

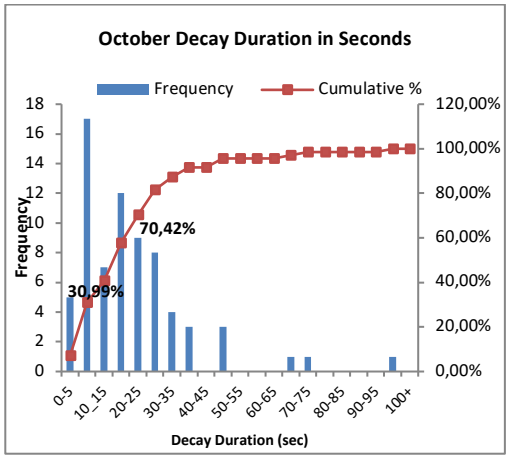

(a)

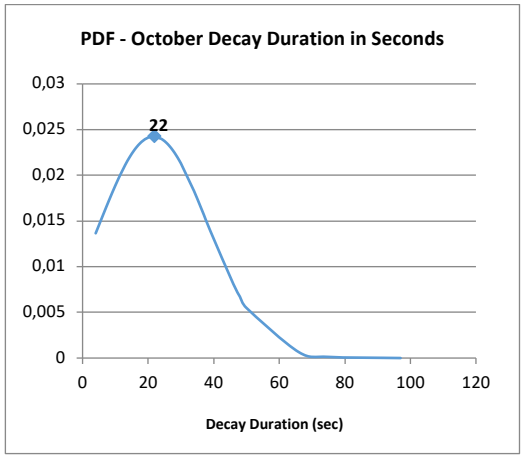

(b)

Fig. 13. October GHI decay duration values in seconds (a) CDF and Frequency (b) PDF

Table 1. Comparison of the GHI analysis results for the different months of the study

	January	**April**	**July**	**October**	**Normalized for the 4 months**
Most frequent value of the GHI relative % change	70-80	60-70	70-80	70-80	70-80
Most frequent GHI decay duration time in seconds	10-5	5-10	10-15	5-10	10-15

4.3. Meteorological parameters analysis results

Fig. 15 to Fig. 19 depict the analysis of the CMS meteorological parameters. The average cloud speeds for the 4 months January, April, July, and October of the year 2013 were combined as a representative of the 4 seasons of the year 2013. Frequency, CDF, and PDF of the cloud average speed are calculated and plotted in Fig. 15. It is observed that the most frequent average speed is 5 to 10 ft/sec (3.41 to 6.81 mph). It is also noticed from Fig. 15(a) that the mean cloud speed is less than or equal to 15 ft/sec for 88.61% of the time. The mean cloud speed with the highest PDF is 10 ft/sec (6.81 mph), as shown in Fig. 15(b). Fig. 16 presents the clouds gusts analysis for the 4 months. Fig. 16(a) shows that the dominant clouds gust falls in the range of 35-40 ft/sec (23.86 - 27.27mph). It is observed that for 70.7% of the time the clouds gust is less than or equal to 40 ft/sec (27.27mph). The cloud gust with the highest PDF is 36 ft/sec (24.54 mph).

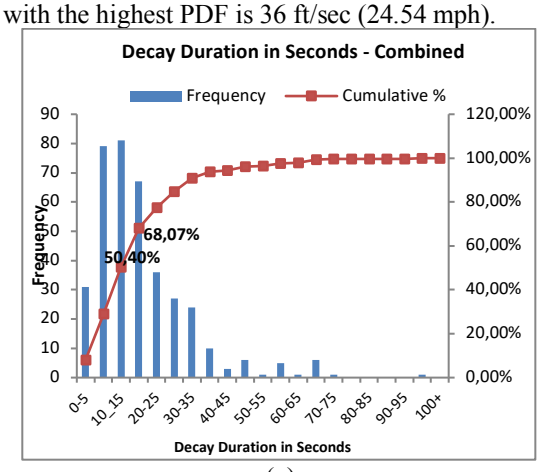

(a)

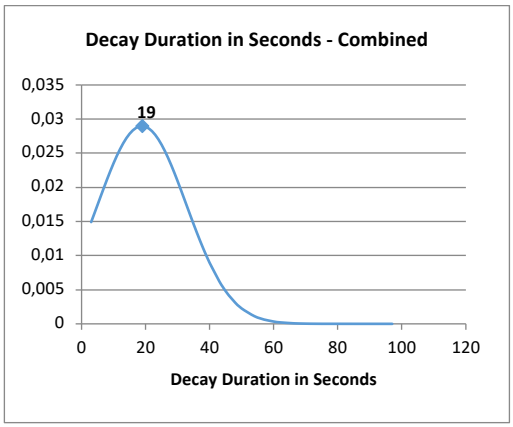

(b)

Fig. 14. The four months combined GHI decay duration values in seconds (a) CDF and Frequency (b) PDF

Fig. 17 shows the cloud width analysis for the 4 months as per the definition of the cloud width elaborated in Section 3.3. The most frequent cloud width is in the range of 100 -200 feet. For 79.18 % of the time the cloud width is less than or equal to 300 feet. The cloud width with the highest PDF is 220.5 ft. The time interval between two consecutive clouds is the time taken for the GHI value to change from GHI_k value to the consecutive drop in the GHI value as shown in Fig. 4. Fig. 18 depicts the analysis for the time interval between 2 consecutive clouds for the 4 months combined. The most frequent time between 2 successive clouds is in the range of 10 to 20 seconds. The interval between 2 successive clouds is less than or equal to 30 seconds for 79.79% of the time. The

interval that has the highest PDF value is 21 seconds between successive clouds.

The number of clouds per hour is analysed in Fig. 19. The most frequent number of clouds per hour is 5 clouds or less. The number of clouds is less than or equal to 10 clouds per hour for 70.83% of the time. The number of clouds per hour that has the highest PDF value is 8 clouds per hour. Table 2 presents a comparison of the meteorological parameters analysis results.

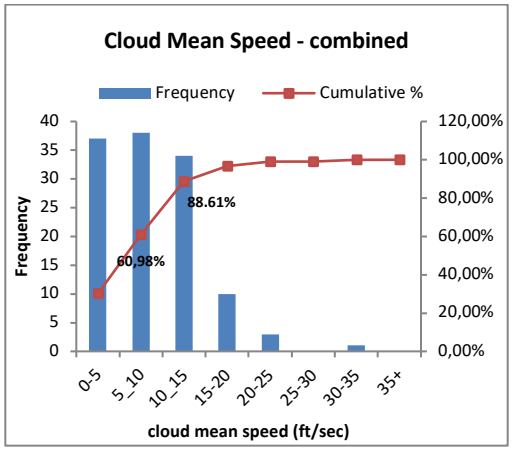

(a)

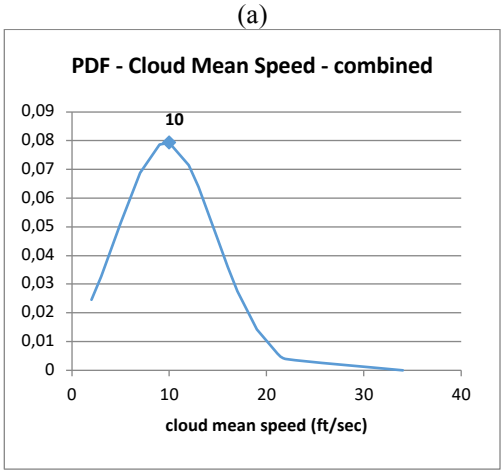

(b)

Fig. 15. The cloud mean speed in ft/sec (a) CDF and Frequency (b) PDF

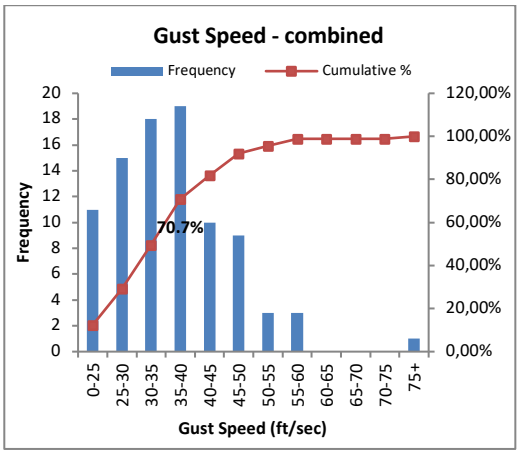

(a)

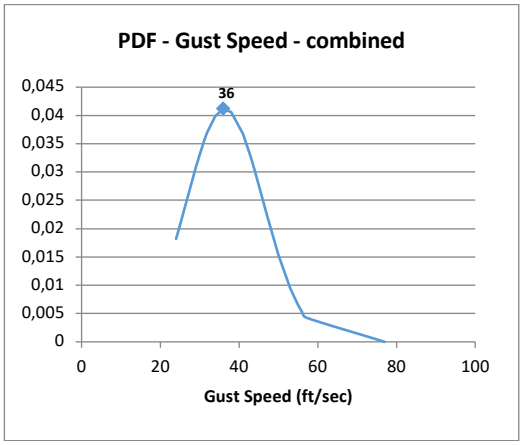

(b)

Fig. 16. The cloud gust speed in ft/sec (a) CDF and Frequency (b) PDF

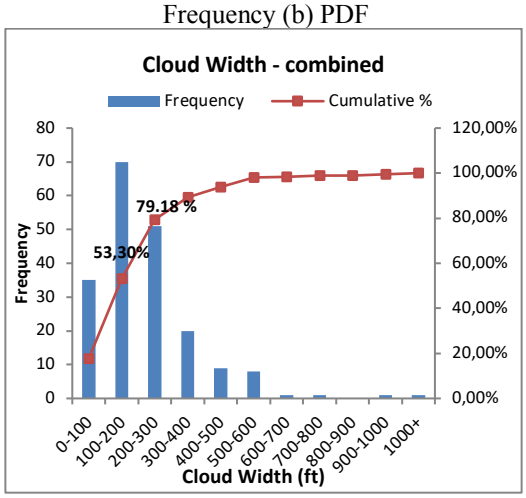

(a)

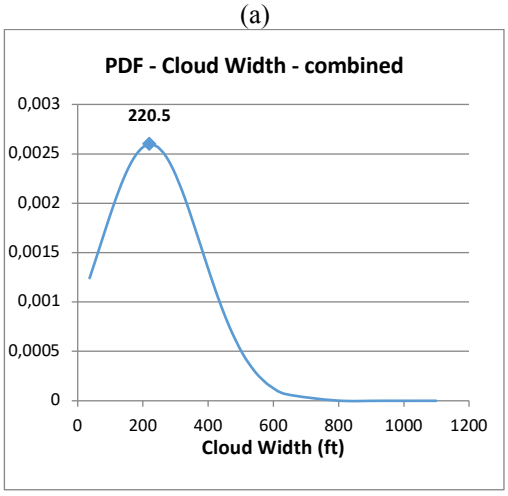

(b)

Fig. 17. The clouds width in ft (a) CDF and Frequency (b) PDF

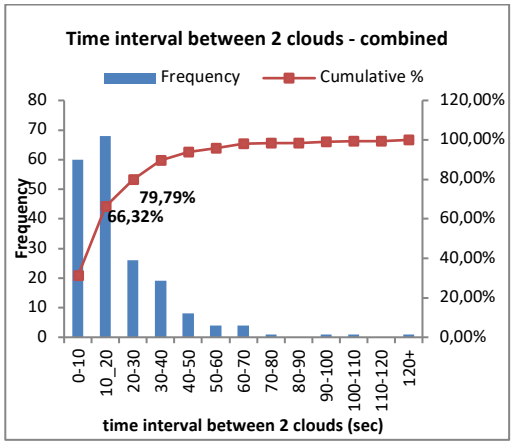

(a)

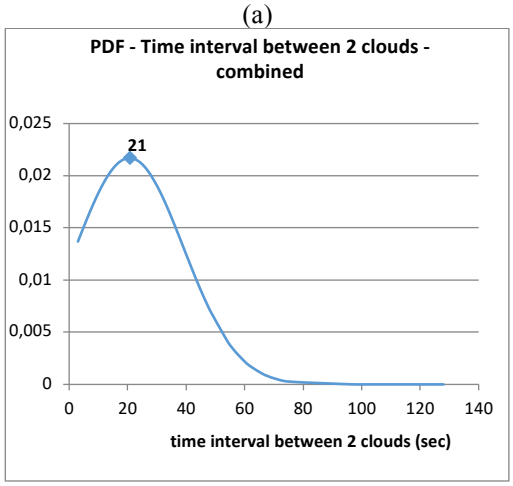

(b)

Fig. 18. The time interval between 2 clouds in seconds (a) CDF and Frequency (b) PDF

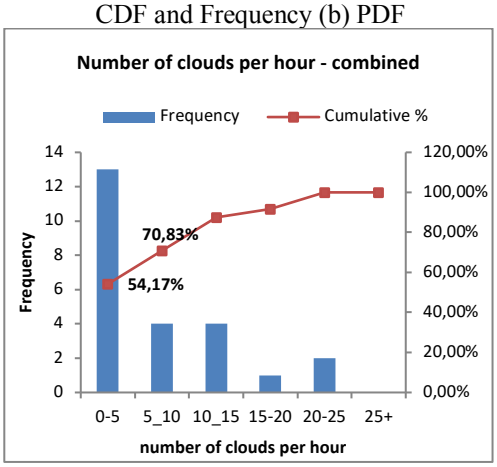

(a)

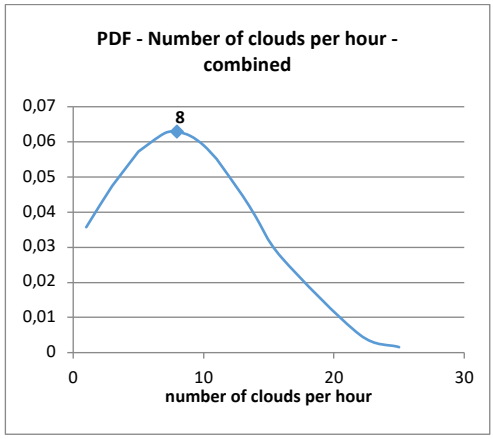

(b)

Fig. 19. The number of clouds passing per hour (a) CDF and Frequency (b) PDF

Table 2. Comparison of the meteorological parameters analysis results

	Normalized for the 4 months
Most frequent average cloud speed in ft/sec	5-10
Most frequent clouds gust falls in ft/sec	35-40
Most frequent cloud width in feet	100-200
Most frequent time between 2 successive clouds in seconds	10-20
Most frequent number of clouds per hour	5 clouds or less

5. Conclusion

Accurate simulation of clouds, which are the key reason of variability in the irradiance received by PV generators, is of interest due to the escalating growth in solar resources implemented worldwide. This paper introduces a statistical analysis of the received irradiance by a real PV plant as well as the meteorological conditions/parameters surrounding the PV arrays. The meteorological data analyzed include the speed of clouds, number of clouds passing, width of the clouds, and the time interval between consecutive clouds.

One objective of this study is to determine the parameter values needed by a Cloud Motion Simulator (CMS), which is a software that simulates the repeated passage of clouds over an electric power system model with PV generation. The CMS simulates the effects of cloud shadows on PV systems, and the consequent voltage fluctuations in a quasi-steady-state fashion. For the relative % change in GHI values, results showed that July has the worst GHI relative % change which is equal to 80% or less for 98.59% of the , and April has the lowest value for GHI relative % change among the 4 months, which is 70%, or less for 82.64% of the time. The relative change of GHI for the 4 months combined is 70% or less for 63.32% of the time. For the GHI decay duration analysis results, it is noted that the most frequent decay duration time for January and July is in the range of 10 to 15 seconds, whereas for April and October it is in the range of 5 to 10 seconds. Moreover, the GHI decay duration is equal to 20 seconds or less for 68.07% of the time for the 4 months combined. The meteorological parameters analysis results for the 4 months cobined showed that: The most frequent average cloud speed is 5 to 10 ft/sec (3.41 to 6.81 mph). The mean cloud speed is less than or equal to 15 ft/sec for 88.61% of the time. The cloud gusts analysis for the 4 months showed that the dominant cloud gust falls in the range of 35-40 ft/sec (23.86 - 27.27mph). The most frequent cloud width is in the range of 100-200 feet. The most frequent time between 2

successive clouds is in the range of 10 to 20 seconds. The most frequent number of clouds per hour is 5 clouds or less. These parameters are to be fed to the CMS which is the software that simulates the repeated passage of clouds over a distribution model and interconnected PV, to study the effects of cloud shadows on the PV system output, and the consequent voltage fluctuations. The results of this analysis enable further studies on the characterization of the uncertainties associated with PV generation.

References

[1] H. E. Murdock, D. Gibb, T. André, F. Appavou, A. Brown, B. Epp, et al., "Renewables 2019 Global Status Report," 2019.

[2] M. Banja and M. Jégard, "An Analysis of Capacity Market Mechanism for Solar Photovoltaics in France," International Journal of Smart Grid-ijSmartGrid, vol. 3, pp. 10-18, 2019.

[3] N. K. Kasim, H. H. Hussain, and A. N. Abed, "Performance Analysis Of Grid-Connected CIGS PV Solar System And Comparison with PVsyst Simulation Program," INTERNATIONAL JOURNAL of SMART GRID, vol. 3, 2019.

[4] A. G. Alkholidi and H. Hamam, "Solar Energy Potentials in Southeastern European Countries: A Case Study," International Journal of Smart Grid-ijSmartGrid, vol. 3, pp. 108-119, 2019.

[5] M. R. Maghami, H. Hizam, C. Gomes, M. A. Radzi, M. I. Rezadad, and S. Hajighorbani, "Power loss due to soiling on solar panel: A review," Renewable and Sustainable Energy Reviews, vol. 59, pp. 1307-1316, 2016.

[6] H. A. Kazem and M. T. Chaichan, "Experimental analysis of the effect of dust's physical properties on photovoltaic modules in Northern Oman," Solar Energy, vol. 139, pp. 68-80, 2016.

[7] M. Firoozzadeh, A. Shiravi, and M. Shafiee, "Experimental Study on Photovoltaic Cooling System Integrated With Carbon Nano Fluid," Journal of Solar Energy Research, vol. 3, pp. 287-292, 2018.

[8] M. Firoozzadeh, A. Shiravi, and M. Shafiee, "An Experimental Study on Cooling the Photovoltaic Modules by Fins to Improve Power Generation: Economic Assessment," Iranian (Iranica) Journal of Energy & Environment, vol. 10, pp. 80-84, 2019.

[9] D. C. Jordan and S. R. Kurtz, "Photovoltaic degradation rates—an analytical review," Progress in photovoltaics: Research and Applications, vol. 21, pp. 12-29, 2013.

[10] C. K. Kim, H.-G. Kim, Y.-H. Kang, C.-Y. Yun, and S. Y. Kim, "Probabilistic prediction of direct normal irradiance derived from global horizontal irradiance over the Korean Peninsula by using Monte-Carlo simulation," Solar Energy, vol. 180, pp. 63-74, 2019.

[11] S. Halilovic, J. M. Bright, W. Herzberg, and S. Killinger, "An analytical approach for estimating the global horizontal from the global tilted irradiance," Solar Energy, vol. 188, pp. 1042-1053, 2019.

[12] E. Scolari, F. Sossan, M. Haure-Touzé, and M. Paolone, "Local estimation of the global horizontal irradiance using an all-sky camera," Solar Energy, vol. 173, pp. 1225-1235, 2018.

[13] W. Zhang, W. Kleiber, A. R. Florita, B.-M. Hodge, and B. Mather, "Modeling and Simulation of High-Frequency Solar Irradiance," IEEE Journal of Photovoltaics, vol. 9, pp. 124-131, 2018.

[14] M. Colak, M. Yesilbudak, and R. Bayindir, "Forecasting of Daily Total Horizontal Solar Radiation Using Grey Wolf Optimizer and Multilayer Perceptron Algorithms," in 2019 8th International Conference on Renewable Energy Research and Applications (ICRERA), 2019, pp. 939-942.

[15] M. Colak, M. Yesilbudak, and R. Bayindir, "Very Short-Term Estimation of Global Horizontal Irradiance Using Data Mining Methods," in 2018 7th International Conference on Renewable Energy Research and Applications (ICRERA), 2018, pp. 1472-1476.

[16] H. Rezk, M. R. Gomaa, and M. A. Mohamed, "Energy Performance Analysis of On-Grid Solar Photovoltaic System-a Practical Case Study," International Journal of Renewable Energy Research (IJRER), vol. 9, pp. 1292-1301, 2019.

[17] M. Ueshima, T. Babasaki, K. Yuasa, and I. Omura, "Examination of Correction Method of Long-term Solar Radiation Forecasts of Numerical Weather Prediction," in 2019 8th International Conference on Renewable Energy Research and Applications (ICRERA), 2019, pp. 113-117.

[18] R. Al-Hajj, A. Assi, and M. M. Fouad, "A predictive evaluation of global solar radiation using recurrent neural models and weather data," in 2017 IEEE 6th International Conference on Renewable Energy Research and Applications (ICRERA), 2017, pp. 195-199.

[19] R. Yan and T. K. Saha, "Voltage variation sensitivity analysis for unbalanced distribution networks due to photovoltaic power fluctuations," IEEE Transactions on Power Systems, vol. 27, pp. 1078-1089, 2012.

[20] Z. Chen, S. Che, Y. Xu, and D. Yin, "Prediction Method of PV Output Power Based on Cloud Model," The Journal of Engineering, vol. 2017, pp. 1519-1523, 2017.

[21] D. Zhao, M. Qian, D. Wang, Y. Liu, L. Zhu, S. Bao, et al., "Impacts of photovoltaic power variation under clouds and LVRT tield test on central power grid of Tibet," in 2017 IEEE Conference on Energy Internet and Energy System Integration (EI2), 2017, pp. 1-5.

[22] N. Kebir and M. Maaroufi, "Predictive evaluation of cloud motion impact on a medium voltage solar PV power system output," in 2015 3rd International Renewable and Sustainable Energy Conference (IRSEC), 2015, pp. 1-6.

[23] J. Krata, T. K. Saha, and R. Yan, "Large scale photovoltaic system and its impact on distribution network in transient cloud conditions," in 2015 IEEE Power & Energy Society General Meeting, 2015, pp. 1-5.

[24] M. Yue and X. Wang, "Assessing cloud transient impacts on grid with solar and battery energy systems," in 2013 IEEE 39th Photovoltaic Specialists Conference (PVSC), 2013, pp. 2348-2353.

[25] I. Vamvakas, V. Salamalikis, and A. Kazantzidis, "Evaluation of enhancement events of global horizontal irradiance due to clouds at Patras, South-West Greece," Renewable Energy, 2019.
[26] D. Pepe, G. Bianchini, and A. Vicino, "Model estimation for solar generation forecasting using cloud cover data," Solar Energy, vol. 157, pp. 1032-1046, 2017.
[27] M. Jazayeri, K. Jazayeri, and S. Uysal, "Generation of spatially dispersed irradiance time-series based on real cloud patterns," Solar Energy, vol. 158, pp. 977-994, 2017.
[28] P. Tzoumanikas, E. Nikitidou, A. Bais, and A. Kazantzidis, "The effect of clouds on surface solar irradiance, based on data from an all-sky imaging system," Renewable Energy, vol. 95, pp. 314-322, 2016.
[29] Z. K. Pecenak, F. A. Mejia, B. Kurtz, A. Evan, and J. Kleissl, "Simulating irradiance enhancement dependence on cloud optical depth and solar zenith angle," Solar Energy, vol. 136, pp. 675-681, 2016.
[30] R. C. de Andrade and C. Tiba, "Extreme global solar irradiance due to cloud enhancement in northeastern Brazil," Renewable energy, vol. 86, pp. 1433-1441, 2016.
[31] R. Tapakis and A. Charalambides, "Enhanced values of global irradiance due to the presence of clouds in Eastern Mediterranean," Renewable energy, vol. 62, pp. 459-467, 2014.
[32] BNL. NSERC, a multi-purpose research facility on the Brookhaven campus. Available: https://www.bnl.gov/energy/NSERC/
[33] K. Rahimi, R. Broadwater, S. Omran, and M. Dilek, "Quasi-Steady-State computation of voltage flicker with cloud motion simulator," in 2017 IEEE Power and Energy Conference at Illinois (PECI), 2017, pp. 1-8.
[34] K. Rahimi, S. Omran, M. Dilek, and R. Broadwater, "Computation of Voltage Flicker with Cloud Motion Simulator," IEEE Transactions on Industry Applications, vol. 54, pp. 2628-2636, 2017.
[35] J. Smith, M. Rylander, L. Rogers, and R. Dugan, "It's all in the plans: Maximizing the benefits and minimizing the impacts of DERs in an integrated grid," IEEE Power and Energy Magazine, vol. 13, pp. 20-29, 2015.
[36] M. Rylander and J. Smith, "Stochastic analysis to determine feeder hosting capacity for distributed solar PV," EPRI Technical Report 1026640, 2012.
[37] K. B. a. A. Kher. (January). Seasons: Meteorological and Astronomical. Available: https://www.timeanddate.com/calendar/aboutseasons.html